machines

MDPI

Article

Robust Trajectory Control of Underactuated Ball and Plate System Using Continuous Full-Order Sliding Mode Controller

Muhammad Haroon Osama [1], Kamal Rsetam [2], Zhenwei Cao [1,*] and Zhihong Man [1]

[1] Faculty of Science, Engineering and Technology, Swinburne University of Technology, Melbourne 3122, Australia; mosama@swin.edu.au (M.H.O.)
[2] Department of Automated Manufacturing, Al Khwarizmi College of Engineering, University of Baghdad, Baghdad 10071, Iraq; krsetam@kecbu.uobaghdad.edu.iq
* Correspondence: zcao@swin.edu.au

Abstract

The stabilization performance of an underactuated ball and plate system (BPS) is significantly degraded by nonlinear dynamics, parameter variations, and external disturbances. This manuscript proposes a robust full-order continuous sliding mode control (FOCSMC) technique to achieve high stabilization performance and enhance the disturbance rejection capability of the BPS. First, the nonlinear dynamics of the BPS are formulated in a full-order state–space form that incorporates the dynamics of both the underactuated ball and the actuated servo motor. Second, two state differentiators (SDs) are introduced to reconstruct the unavailable state variables required for controller implementation. By avoiding direct high-order differentiation of measured signals, the proposed differentiators reduce noise sensitivity and improve practical realizability. Based on the estimated states, a continuous full-order sliding manifold is constructed to guarantee asymptotic convergence of the closed-loop system states while reducing the chattering phenomenon inherently associated with conventional sliding mode control (SMC) schemes. A Lyapunov-based stability analysis is performed to establish asymptotic convergence. Finally, comparative simulation and experimental studies under nominal conditions, parameter variations, external disturbances, and two-dimensional circular trajectory tracking demonstrate that the proposed FOCSMC consistently outperforms the hierarchical SMC (HSMC) and the continuous SMC (CSMC) schemes. In particular, the root mean square (RMS) and the maximum (MAX) of the tracking error are, respectively, 0.5653 cm and 1.9461 cm, which are experimentally achieved under the impact of the disturbances, confirming the effectiveness and practical applicability of the proposed scheme.

Keywords: ball and plate system (BPS); full-order continuous sliding mode control (FOCSMC); state differentiator (SD); robustness; chattering reduction; experimental validation

Check for updates

Academic Editor: Zafer Bingul

Received: 18 June 2026
Revised: 23 July 2026
Accepted: 31 July 2026
Published: 3 August 2026

Copyright: © 2026 by the authors. Licensee MDPI, Basel, Switzerland. This article is an open access article distributed under the terms and conditions of the Creative Commons Attribution (CC BY) license.

1. Introduction

Underactuated mechanical systems (UMSs) have attracted significant research attention in modern control engineering due to their nonlinear dynamics and wide range of practical applications applications in robotics [1], aerospace systems, and precision motion platforms [2,3]. Among these systems, the ball and plate system (BPS) has emerged as a well established experimental platform for validating advanced nonlinear control algorithms [4]. The BPS consists of a rigid plate actuated by servo motors that regulate the motion of a freely rolling ball on its surface. Although the mechanical structure appears simple, the

system exhibits highly nonlinear and strongly coupled dynamics resulting from the rolling motion of the ball and the actuator dynamics. Owing to these characteristics, the BPS has been widely used to evaluate robust nonlinear control strategies, as demonstrated in [5].

Despite its widespread use in control research, the BPS poses several control challenges due to its underactuated nature. The ball position cannot be controlled directly. Instead, its motion is influenced indirectly through the inclination angles of the plate generated by the servo motors, which leads to strong state coupling and nonlinear dynamics [5]. Furthermore, the coupled interaction between the ball dynamics and the actuator dynamics increases the system order and further complicates the control design process. In practical scenarios, system uncertainties, parametric variations, unmodeled dynamics, and external disturbances also degrade the control performance [6–8]. Consequently, achieving accurate and robust stabilization of the BPS remains a nontrivial control problem.

To address the challenges associated with nonlinear underactuated systems, various control techniques have been proposed in the literature. These approaches include feedback linearization [9], adaptive control [10], backstepping control [11], model predictive control [12,13], visual servoing tracking control [14], Python script-based control [15], intelligent control techniques based on fuzzy logic [16] and neural networks [17], state filtered disturbance rejection control [18], and multilayer neuroadaptive reinforcement learning [19]. Although these methods have demonstrated excellent disturbance rejection and tracking performance, they generally involve relatively complex control structures and higher computational requirements. In the context of the BPS, many nonlinear and robust control techniques are reported in the literature, including classical sliding mode control [20]and multisurface control designs [4]. Among these methods, sliding mode control (SMC) has received considerable attention due to its strong robustness against matched disturbances and modeling uncertainties [21–24]. Owing to these properties and its relatively simple implementation, SMC has been widely applied to many nonlinear UMSs such as flexible joint robots, unmanned surface vehicles, and other nonholonomic systems [5,7,25].

Nonetheless the SMC methods have some limitations that restrict their practical implementation; these limitations include control chattering, which arises due to the discontinuous switching term available in traditional SMC design. This chattering can excite unmodeled dynamics, induce excessive wear in actuators, and cause undesirable oscillations [6,26]. Moreover, many existing SMC approaches require high-order derivatives of system states or precise knowledge of uncertainty bounds, which increases the sensitivity to measurement noise and complicates the implementation process [7,27]. In the available literature, an integral SMC is proposed to mitigate chattering and improve convergence, but it leads to complex control structures. Moreover, many SMC-based controllers for the BPS are developed using reduced-order models, hierarchical SMC [28], with limited focus on underactuated dynamics and system uncertainties. These limitations indicate the necessity for developing an SMC framework that ensures chattering reduction, robustness, and implementation simplicity for the BPS.

Motivated by the above challenges, this paper proposes a robust full-order continuous sliding mode controller (FOCSMC) for the stabilization of an underactuated BPS. The proposed framework integrates a continuous full-order sliding mode controller with two state differentiators. This integration eliminates the need for the direct high-order differentiation of measured signals and the model information, reduces the noise sensitivity, and improves the practical implementation. It also provides disturbance rejection ability and accurate trajectory tracking. Compared with recent approaches, the proposed method offers a simpler controller design with a lower computational burden while preserving

disturbance rejection and accurate trajectory tracking. The main contributions of this article are summarized as follows:

1. The underactuated BPS dynamics are transformed into canonical form through a flatness approach; as a result, mismatched disturbance is transferred into matched disturbance. The resulting configuration eases the controller synthesis, where system states are in the form of chain of derivatives and control input, and nonlinear system dynamics along with disturbance appear on the highest channel.
2. A continuous full-order sliding mode control (FOCSMC) framework is newly developed for the underactuated BPS. The proposed controller reduces chattering while maintaining robustness against model uncertainties and external disturbances.
3. A cascade state differentiator structure is employed to estimate the unavailable states required for controller implementation. The proposed differentiators eliminate the direct high-order differentiation of measured signals and reduce the noise sensitivity.
4. A Lyapunov-based stability analysis is carried out to guarantee asymptotic convergence and closed-loop stability. The proposed controller is subsequently evaluated through simulation and real-time experimental investigations on a laboratory-scale ball and plate system.

The proposed controller is validated through comparative simulation and real-time experiments against the HSMC and the CSMC methods. The results demonstrate improved transient performance, significant chattering reduction, and enhanced robustness to uncertainties.

The rest of the paper is organized as follows: Section 2 introduces the system modeling. Section 3 describes the state differentiator design, controller synthesis, and stability analysis. Section 4 presents the simulation and experimental validations. Conclusions are drawn in Section 5.

2. Mathematical Formulation of BPS

This section provides a description and dynamic modeling of a BPS.

2.1. Description of a BPS

The side view representation of the BPS is illustrated in Figure 1. This hardware platform is widely used as a benchmark experimental setup for validating advanced nonlinear control strategies for UMSs and is manufactured by Quanser [29]. The system consists of a rigid plate actuated by two orthogonal rotary servo motors, which regulate the inclination angles of the plate along the x-axis and y-axis. Its working mechanism involves transmitting the rotational motion generated by the servo motors to control the tilting angle of a plate. The motion of the plate creates a gravitational component along the inclined surface that drives the movement of the ball.

In the configuration shown in Figure 1, θ_m denotes the corresponding servo motor angle responsible for adjusting α the plate orientation. The ball rolls freely on the plate surface, and its position is indirectly controlled through the variation of these inclination angles. Due to this indirect actuation mechanism, the number of control inputs is fewer than the degrees of freedom of the system, which classifies the BPS as a typical underactuated nonlinear mechanical system.

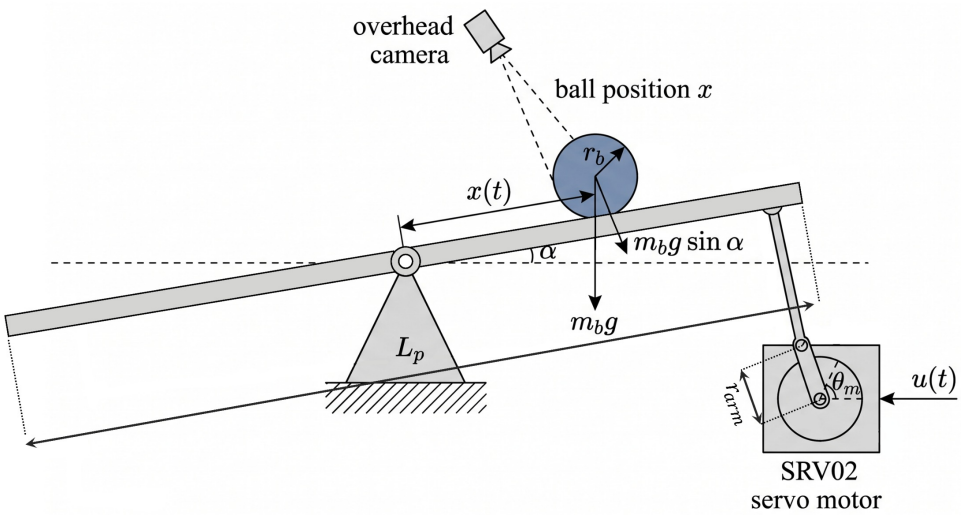

Figure 1. Side view schematic of the underactuated BPS in the x-direction.

2.2. Dynamical Modeling of a BPS

The nonlinear dynamics of the BPS [30] are derived using the Euler–Lagrange formulation. The coupled dynamics of BPS along with servo motor in x-axis can be represented as follows:

$$\ddot{x} = K_{bb} \sin\theta_m + d_1(t), \tag{1}$$

$$\ddot{\theta}_m = -\frac{1}{\tau}\dot{\theta}_m + \frac{K}{\tau}u(t) + d_2(t). \tag{2}$$

with

$$K_{bb} = \frac{2m_b g\, r_{\text{arm}}\, r_b^2}{L_{\text{p}}\,(m_b r_b^2 + J_b)},$$

where x represents the displacement of the ball along the plate, θ_m represents the servo motor angle, $d_1(t)$ and $d_2(t)$ are, respectively, the mismatched and matched external disturbances, and $u(t)$ is the control input voltage. In addition, τ and K are the motor constants, whose values are provided in Table 1. Based on the dynamics described in (1) and (2), the state–space model of the BPS is obtained as follows:

$$\begin{aligned}
\dot{\eta}_1 &= \eta_2, \\
\dot{\eta}_2 &= f_b(\eta, t) + d_1, \\
\dot{\eta}_3 &= \eta_4, \\
\dot{\eta}_4 &= f_m(\eta, t) + bu(t) + d_2.
\end{aligned} \tag{3}$$

with

$$f_b(\eta, t) = K_{bb} \sin\eta_3 \text{ and } f_m(\eta, t) = -\frac{1}{\tau}\eta_4.$$

Here, $\eta = [\eta_1 = x;\ \eta_2 = \dot{x};\ \eta_3 = \theta_m;\ \eta_4 = \dot{\theta}_m]^T$ is the state vector, which consists of the BPS variables. Moreover, f_b represents the nonlinear dynamics of the ball subsystem, $f_m(\eta, t)$ is the dynamics of the servo motor subsystem, and $b = \frac{K}{\tau}$ denotes the corresponding control input constant. The presence of unmatched disturbances in the system dynamics prevents their direct compensation through the control input. To account for this effect, a flatness-based transformation is adopted by selecting the ball position as the flat output and differentiating it up to the fourth order to obtain the input–output representation, consistent with the system's relative degree.

Table 1. BPS nominal parameters.

Parameters	Description	Number
m_b	Ball mass (kg)	0.0030
g	Gravitational constant (m/s^2)	9.8100
r_b	Ball radius (m)	0.0196
r_{arm}	Servo arm radius (m)	0.0330
L_p	Plate length (m)	0.2750
I_b	Ball rotational inertia (kg. m^2)	4.6217×10^{-7}
J_{eq}	Equivalent rotational inertia (kg. m^2)	0.0018
B_{eq}	Equivalent viscous damping coefficient (N. m. s/rad)	0.0150
K	Servo motor gain (rad/(A. s))	1.5286

In contrast to conventional coordinate transformations, the system states in this work retain their physical interpretation, where $\eta_1(t) = y(t)$, $\eta_2(t) = \dot{y}(t)$ refer to the ball position and velocity, respectively, while the higher-order derivatives of the output are obtained through successive differentiation of the nonlinear dynamics. This procedure results in a fourth-order affine canonical form in which the control input explicitly appears in the highest-order derivative, enabling the treatment of disturbances within a matched framework. To facilitate the controller design, the ball position is selected as the flat output of the system. Let the output be defined as

$$y = x_1 = \eta_1. \tag{4}$$

Using the state–space model given in (3), the successive derivatives of the output can be obtained as

$$\begin{aligned} \dot{y} &= \dot{x}_1 = x_2 = \eta_2, \\ \ddot{y} &= \dot{x}_2 = x_3 = \dot{\eta}_2 = f_b(\eta, t) + d_1, \\ y^{(3)} &= \dot{x}_3 = x_4 = \ddot{\eta}_2 = \dot{f}_b(\eta, t) + \dot{d}_1, \\ y^{(4)} &= \dot{x}_4 = \dddot{\eta}_2 = \ddot{f}_b(x, t) + \ddot{d}_1. \end{aligned} \tag{5}$$

From (5), the first and second derivatives of the nonlinear ball and plate subsystem function are as follows:

$$\begin{aligned} f_b &= K_{bb} \sin \eta_3 \\ \dot{f}_b &= K_{bb} \dot{\eta}_3 \cos \eta_3 = K_{bb} \eta_4 \cos \eta_3 \\ \ddot{f}_b &= K_{bb}[\dot{\eta}_4 \cos \eta_3 - \eta_4^2 \sin \eta_3] = K_{bb}[(f_m + bu + d_2) \cos \eta_3 - \eta_4^2 \sin \eta_3] \\ &= K_{bb}[f_m \cos \eta_3 + b \cos \eta_3 u + d_2 \cos \eta_3 - \eta_4^2 \sin \eta_3] \\ &= K_{bb}(f_m \cos \eta_3 - \eta_4^2 \sin \eta_3) + K_{bb} b \cos \eta_3 u + K_{bb} d_2 \cos \eta_3 \end{aligned} \tag{6}$$

Based on (6), the signal of $\dot{x}_4$ in (5) becomes

$$\dot{x}_4 = f(x, t) + Bu(t) + \delta(t) \tag{7}$$

with

$$f(x, t) = K_{bb}(f_m \cos \eta_3 - \eta_4^2 \sin \eta_3); B = K_{bb} b \cos \eta_3; \text{ and } \delta = K_{bb} d_2 \cos \eta_3 + \ddot{d}_1$$

Assumption 1. *The disturbances $d_1(t)$ and $d_2(t)$ in (3) are sufficiently smooth and bounded over each operating interval such that the derivatives required by the coordinate transformation in (4–6)*

exist and remain bounded. Consequently, the lumped disturbance $\delta(t)$ in (7) is bounded by the following expression $|\delta(t)| \leq \bar{\delta}$, where $\bar{\delta} > 0$ is the constant.

Remark 1. *The differentiable disturbances of $d_1(t)$ and $d_2(t)$ only appear in the mathematical model of the BPS in (7), and they are not necessarily required for our control procedure. We only need the bound of the total disturbance of $\delta(t)$ as assumed in Assumption 1 to guarantee the robustness and stability of the BPS.*

Now, using (7), the BPS dynamics in (5) can be rewritten in the following affine canonical form:

$$\begin{aligned} \dot{x}_1 &= x_2, \\ \dot{x}_2 &= x_3, \\ \dot{x}_3 &= x_4, \\ \dot{x}_4 &= f_0(x,t) + B_0 u(t) + D(x,t). \end{aligned} \tag{8}$$

with

$$\begin{aligned} f(x,t) &= f_0(x,t) + \Delta f(x,t), \\ B &= B_0 + \Delta B \\ D(x,t) &= \Delta f(x,t) + \Delta B\, u + \delta(t) \end{aligned}$$

where $f_0(x,t)$ and B_0 denote the nominal dynamics, while $\Delta f(x,t)$ and ΔB represent the uncertainties. The term $D(x,t)$ denotes the lumped modeling uncertainties, higher-order nonlinearities, and external disturbances.

3. Proposed Controller Design

This section presents the development of the proposed control strategy. First, the state differentiators are introduced, followed by the design of the FOCSMC. Figure 2 shows the block diagram of the designed FOCSMC methodology with two SDs.

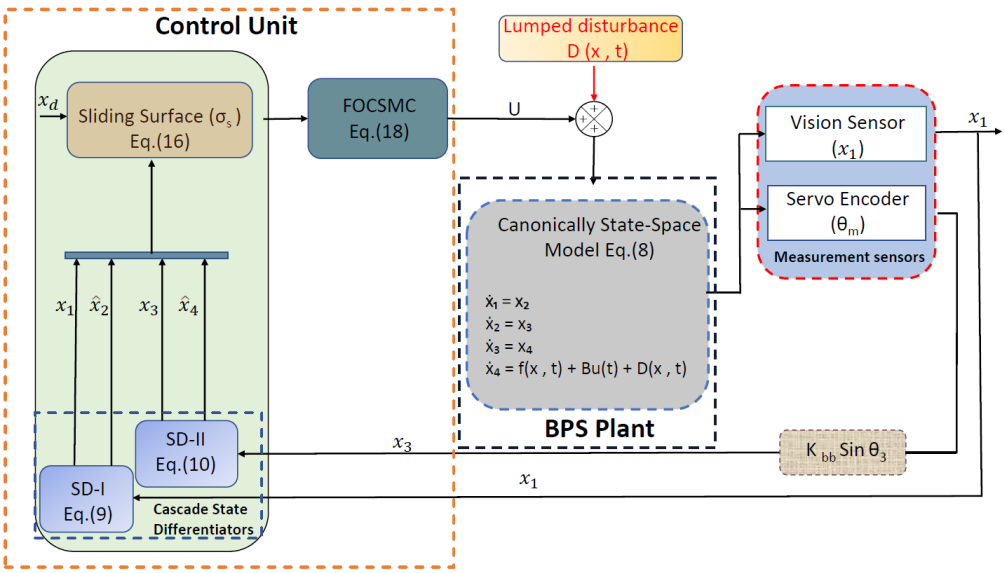

Figure 2. Block diagram of the proposed FOCSMC method with SDs.

3.1. State Differentiators Design

To facilitate controller implementation, two state differentiators [31] are developed to estimate the unavailable system states in (8), as follows:

$$\dot{\hat{x}}_1 = \hat{x}_2 + \gamma_1(x_1 - \hat{x}_1)$$
$$\dot{\hat{x}}_2 = \gamma_2(x_1 - \hat{x}_1) \tag{9}$$
$$\dot{\hat{x}}_3 = \hat{x}_4 + \kappa_1(x_3 - \hat{x}_3)$$
$$\dot{\hat{x}}_4 = \kappa_2(x_3 - \hat{x}_3) \tag{10}$$

with

$$x_3 = \dot{\eta}_2 = K_{bb} \sin \eta_3 = K_{bb} \sin \theta.$$

The states x_1 and x_3 correspond to the available ball position and plate angle, respectively. These signals are directly measured from the vision system and servo encoder of the BPS. The remaining states, $\hat{x}_2$ and $\hat{x}_4$ are not directly measurable and are therefore estimated using the SD introduced in (9) and (10). Furthermore, γ_i and κ_i for $i = 1, 2$ represent the differentiator gains that are selected according to the desired characteristic polynomials given by [32]

$$P_1(s) = s^2 + \gamma_1 s + \gamma_2 = (s + \omega_{d1})^2 \tag{11}$$

$$P_2(s) = s^3 + \kappa_1 s + \kappa_2 = (s + \omega_{d2})^2. \tag{12}$$

The differentiator gains $\omega_{di} > 0$ for i = 1, 2 are selected such that all observer poles of the provided characteristic polynomials in (11) and (12) are placed in the left half of the complex plane, hence ensuring stable estimation dynamics. The parameters can determine the bandwidths of both SD (9) and (10), respectively, and are chosen as $\omega_{di} > 0$, for i = 1, 2.

Thus, the two SDs are employed to estimate the unavailable states x_2 and x_4, which are required for the implementation of the proposed control law presented in the subsequent section.

Remark 2. *Since the motor angle η_3 is obtained from the servo encoder, it may be affected by measurement noise. In the proposed method, the required derivatives are reconstructed using the cascaded state differentiator in (9) and (10) rather than the use of direct numerical differentiation. Consequently, the proposed differentiator exhibits the merits of filtering characteristics, which attenuate high-frequency measurement noise while providing smooth state estimates to the designed controller. Furthermore, the differentiator bandwidth in (11) and (12) is selected to ensure a better trade-off between estimation accuracy and noise sensitivity.*

3.2. Control Design and Stability Analysis

Next, the tracking error variables are defined as

$$e_1 = x_1 - x_d,$$
$$e_2 = x_2 - \dot{x}_d,$$
$$e_3 = x_3 - \ddot{x}_d,$$
$$e_4 = x_4 - x_d^{(3)} \tag{13}$$

where x_d, $\dot{x}_d$, $\ddot{x}_d$, and $x_d^{(3)}$ denote the desired reference trajectory of the ball and its successive derivatives. Accordingly, the error-state vector is expressed as

$$e = \begin{bmatrix} e_1 & e_2 & e_3 & e_4 \end{bmatrix}^T. \tag{14}$$

Based on (8) and (13), the corresponding tracking error dynamics are obtained as

$$\begin{aligned} \dot{e}_1 &= e_2, \\ \dot{e}_2 &= e_3, \\ \dot{e}_3 &= e_4, \\ \dot{e}_4 &= \dot{e}_4 = f_0(x,t) + B_0 u(t) + D(x,t) - x_d^{(4)}(t). \end{aligned} \tag{15}$$

Using the error dynamics in (15), the continuous sliding surface can be constructed as follows:

$$\sigma_s(t) = \dot{e}_4 + k_4\hat{e}_4 + k_3 e_3 + k_2\hat{e}_2 + k_1 e_1. \tag{16}$$

Let the tracking errors be defined as

$$e_1 = x_1 - x_d, \quad \hat{e}_2 = \hat{x}_2 - \dot{x}_d, \quad e_3 = x_3 - \ddot{x}_d, \quad \hat{e}_4 = \hat{x}_4 - x_d^{(3)},$$

where $\hat{x}_2$ and $\hat{x}_4$ are obtained by the SDs in (9) and (10), respectively. Moreover, $k_i > 0$ for $i = 1,2,3,4$ denotes control parameters to be designed, such that the polynomial equation $p_c(s)$ in the complex variable s is defined as

$$p_c(s) = s^4 + k_4 s^3 + k_3 s^2 + k_2 s + k_1, \tag{17}$$

which has all its roots located in the left half of the complex plane, thereby ensuring Hurwitz stability. Based on the defined error dynamics, the sliding variable is constructed in (16), and the corresponding control input is formulated by

$$u = -B_0^{-1}(u_{eq} + u_{sw}) \tag{18}$$

$$u_{eq} = f_0(x,t) + k_4\hat{e}_4 + k_3 e_3 + k_2\hat{e}_2 + k_1 e_1 - x_d^{(4)}(t) \tag{19}$$

$$u_{sw} = K\int_0^t \operatorname{sgn}(\sigma)dt \tag{20}$$

where u_{eq} and u_{sw} correspond to the equivalent and switching control actions, respectively, and $K > 0$ is selected to satisfy the reaching condition. Consequently, the closed-loop system states converge asymptotically to their desired trajectories.

Remark 3. *The parameters k_i for ($i = 1,2,3,4$) are selected using a pole-placement approach in (17) to ensure the desired closed-loop dynamics. Specifically, they are assigned as the coefficients of the desired characteristic polynomial in (17) such that all poles lie in the left half of the complex plane, thereby ensuring the stability of the ball on the plate.*

Assumption 2. *The lumped uncertainty and disturbance term D(x,t) appearing in the canonical model (8) is assumed to be continuously differentiable and bounded. Furthermore, its time derivative is bounded such that*

$$|\dot{D}(x,t)| \le \eta, \tag{21}$$

where $\eta > 0$ is a constant.

Theorem 1. *Consider the underactuated BPS described by (8) and the continuous full-order sliding manifold defined in (16). Under Assumption 1, if the control law (18) is applied with switching gain K satisfying $K > \eta$, then all closed-loop signals remain bounded, and σ_s reaches $\sigma_s = 0$. Moreover, the regulation errors e_i, i=1,2,3,4, converge asymptotically to zero.*

Proof 1. Based on (18), the sliding-mode variable in (16) can be written as

$$\begin{aligned}\sigma_s(t) &= \dot{e}_4 + k_4\hat{e}_4 + k_3e_3 + k_2\hat{e}_2 + k_1e_1 \\ &= D(x,t) - K\int_0^t \operatorname{sgn}(\sigma_s)\,dt\end{aligned} \tag{22}$$

Now, the first-order derivative of σ_s in (22) is as follows:

$$\dot{\sigma}_s = \dot{D}(x,t) - K\operatorname{sgn}(\sigma_s). \tag{23}$$

Choose the Lyapunov candidate function as

$$V_\sigma = \frac{1}{2}\sigma_s^2. \tag{24}$$

Differentiating V_σ in (24) with respect to time along the surface dynamics (22) obtains

$$\begin{aligned}\dot{V}_\sigma &= \sigma_s\dot{\sigma}_s \\ &= \sigma_s\Big(-K\operatorname{sgn}(\sigma_s) + \dot{D}(x,t)\Big) \\ &= -K|\sigma_s| + \dot{D}(x,t)\sigma_s \\ &\le -K|\sigma_s| + |\dot{D}(x,t)||\sigma_s| \\ &= -\Big(K - |\dot{D}(x,t)|\Big)|\sigma_s| \\ &\le -(K-\eta)|\sigma_s| \\ &\le -M|\sigma_s| \\ &= -\sqrt{2}\,M\,V_\sigma^{1/2},\end{aligned} \tag{25}$$

where $M = K - \eta > 0$. Therefore, from (25), if the switching gain is selected such that $K > \eta$, then $\dot{V}_\sigma < 0$. Hence, the sliding variable σ_s converges to the sliding manifold $\sigma_s = 0$ in the reaching time T. After the reaching time $t \ge T$, the sliding motion in (16) is maintained at zero, i.e., $(\sigma_s = 0)$. Hence, from (22), the sliding dynamics are described by

$$0 = \dot{e}_4 + k_4\hat{e}_4 + k_3e_3 + k_2\hat{e}_2 + k_1e_1. \tag{26}$$

In the system (26), the estimated tracking errors $\hat{e}_2$ and $\hat{e}_4$ can be expressed by

$$\begin{aligned}\hat{e}_2 &= e_2 - \tilde{e}_2 \\ \hat{e}_4 &= e_4 - \tilde{e}_4.\end{aligned} \tag{27}$$

where $\tilde{e}_2$ and $\tilde{e}_4$ are the estimation error of the signal $\hat{x}_2$ and $\hat{x}_4$ estimated by the SDs in (9) and (10), respectively. Substituting (26) into the dynamics in (26), one obtains

$$\dot{e}_4 + k_4e_4 + k_3e_3 + k_2e_2 + k_1e_1 = \tilde{e}_4 + \tilde{e}_2. \tag{28}$$

Combining the error dynamics and (15) and (28) yields

$$e_1^{(4)} + k_4e_1^{(3)} + k_3\ddot{e}_1 + k_2\dot{e}_1 + k_1e_1 = \tilde{e}_4 + \tilde{e}_2. \tag{29}$$

Since the estimations of the unknown states $\hat{x}_2$ and $\hat{x}_4$ can asymptotically track their true states x_2 and x_4 as the SDs in (9) and (10) aim at, this means that the estimation errors of such states $\tilde{e}_2$ and $\tilde{e}_4$ in (29) satisfy $\lim_{t\to\infty}\tilde{e}_2 = \lim_{t\to\infty}(x_2 - \hat{x}_2) = 0$, and $\lim_{t\to\infty}\tilde{e}_4 = \lim_{t\to\infty}(x_4 - \hat{x}_4) = 0$, respectively. With these results, it can be ensured that the error dynamics in (29) becomes

$$e_1^{(4)} + k_4 e_1^{(3)} + k_3\ddot{e}_1 + k_2\dot{e}_1 + k_1 e_1 = 0. \tag{30}$$

The dynamics in (30) are asymptotically stable when the asymptotic stability of the two observer-error dynamics is achieved. From the above system, it can be derived that the output tracking error satisfies $\lim_{t\to\infty} e_1 = \lim_{t\to\infty}(x_1 - x_d) = 0$. This implies that the tracking errors converge asymptotically to the desired equilibrium point along $\sigma_s = 0$ under the proposed control action. Thus, the system output can track its reference asymptotically, as in $\lim_{t\to\infty} x_1 = x_d$. □

The parameters k_i $(i = 1, 2, 3, 4)$ in (16) and (17) are tuned according to the fourth-order polynomial characteristics as follows:

$$p_c(s) = (s + \omega_c)^4 \tag{31}$$

with

$$[k_1,\, k_2,\, k_3,\, k_4] = [\omega_c^4,\, 4\omega_c^3,\, 6\omega_c^2,\, 4\omega_c], \tag{32}$$

where $\omega_c = 8$ rad/sec represents the proposed controller bandwidth.

Remark 4. *The controller parameters k_i for $(i = 1, 2, 3, 4)$ in (16) and (19) are selected by using a bandwidth-based pole placement approach in (17) and (31). Specifically, the coefficients k_i for $(i = 1, 2, 3, 4)$ of the desired closed-loop characteristic polynomial in (17) are determined to satisfy the Hurwitz stability condition and achieve the desired transient response. These controller parameters are then fine-tuned through simulation and experimental validation to obtain a suitable trade-off between tracking accuracy and noise reduction in the control effort.*

4. Simulations and Experimental Results

The performance of the proposed FOCSMC is evaluated through both numerical simulations and real-time experiments. To provide a comprehensive assessment, two benchmark controllers were first used. CSMC [20] was used to validate the advantages of the proposed scheme in improving regulation performance and reducing chattering. Second, the HSMC [28] investigates the structural capability of the proposed method for underactuated system stabilization. Based on Table 2, the evaluation is conducted under three operating scenarios: nominal conditions, parameter variations, and external disturbances. The objective is to examine the regulation accuracy, robustness, and control effort of the proposed method under different operating conditions.

Table 2. Controller parameters.

Controller	Controller Parameters
Proposed FOCSMC	$\omega_{d1} = 100$ rad/s; $\omega_{d2} = 100$ rad/s; $\omega_c = 8$ rad/s; $K = 1.5$.
Conventional SMC [20]	$C_1 = 100$; $C_2 = 44$; $C_3 = 11$; $\lambda = 10$.
Hierarchical SMC [28]	$Ch_1 = 89.85$; $Ch_2 = 29.34$; $M_p = 5$.

4.1. Simulation Results Analysis

This section evaluates the effectiveness of the proposed FOCSMC through a set of simulation studies designed to represent practical operating scenarios. These tests are

conducted to examine the closed-loop performance and robustness of the proposed control strategy under varying operating conditions. The simulations are carried out in MATLAB/Simulink R2024b on a 64-bit Windows 11 platform equipped with an Intel Core i7-6700 processor operating at 4.00 GHz and 8 GB RAM as shown in Figure 3. A fixed sampling interval of 0.002 s is adopted throughout the simulations. The performance of the proposed controller is assessed through comparisons with the CSMC [20] and HSMC [28].

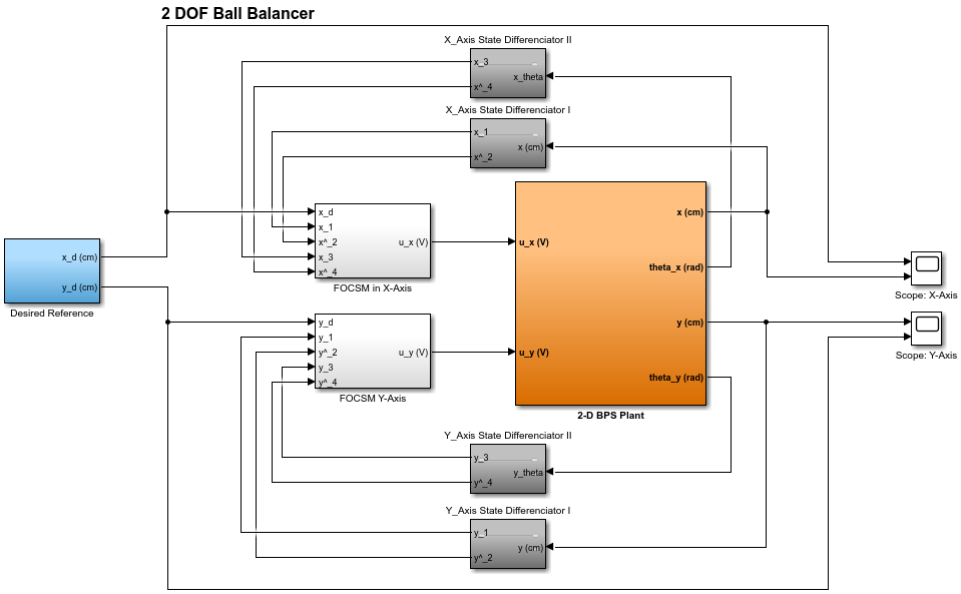

Figure 3. Simulink implementation of the proposed FOCSMC.

Case 1: In the first test, the ball was initialized at (−6 cm) from the center of the plate and regulated to the equilibrium position under nominal operating conditions. The ball position and control input responses are shown in Figure 4a and Figure 4b, respectively.

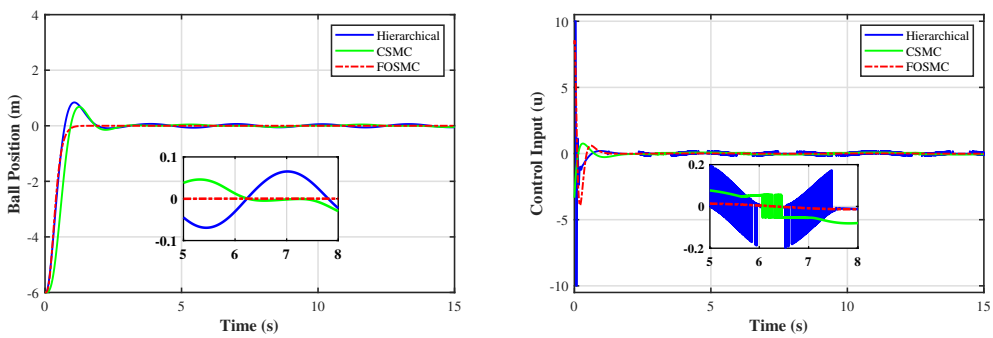

(**a**) (**b**)

Figure 4. Response curves of the BPS with the nominal system parameters (Simulation Case 1): (**a**) Ball position. (**b**) Control input.

As shown in Figure 4a, all controllers successfully regulate the ball position to the origin. However, the proposed FOCSMC achieves a faster settling response with reduced oscillations compared with the HSMC and the CSMC. The corresponding control input in Figure 4b remains smooth and continuous, indicating reduced chattering during the regulation process. The quantitative results reported in Table 3 further validate the effectiveness of the proposed controller. The FOCSMC achieves the lowest RMS and the MAX of 0.00017 cm and 0.00019 cm, respectively, compared with 0.0457 cm and 0.0674 cm for

the HSMC and 0.0324 cm and 0.0460 cm for the CSMC. These results demonstrate the improved regulation accuracy of the proposed approach under nominal conditions.

Table 3. Simulation error analysis in (cm).

Cases	Index	Proposed	HSMC	CSMC
Case 1	RMS	0.00017	0.0457	0.0324
	MAX	0.00019	0.0674	0.0460
Case 2	RMS	0.00018	0.0376	0.0270
	MAX	0.00019	0.1193	0.0349
Case 3	RMS	0.0011	0.0292	0.1408
	MAX	0.0055	0.1440	0.5957

Case 2: In the second test, the robustness of the controllers against parameter uncertainties was evaluated by increasing the ball mass by 10% and the ball radius by 4.4%, resulting in an approximate 20% increase in the ball inertia. The corresponding ball position and control input responses are shown in Figure 5a and Figure 5b, respectively. As shown in Figure 5a, all controllers maintain closed-loop stability under the parameter variations. However, the proposed FOCSMC achieves faster convergence with smaller oscillations around the equilibrium point compared with the HSMC and the CSMC. The corresponding control input in Figure 5b remains smooth and bounded throughout the regulation process. The quantitative results reported in Table 3 further demonstrate the robustness of the proposed controller. The FOCSMC achieves an RMS and the MAX of 0.00018 cm and 0.00019 cm, respectively, whereas the HSMC yields 0.0376 cm and 0.1193 cm, and the CSMC records 0.0270 cm and 0.0349 cm. These results indicate that the proposed controller maintains its regulation performance despite the introduced parameter variations.

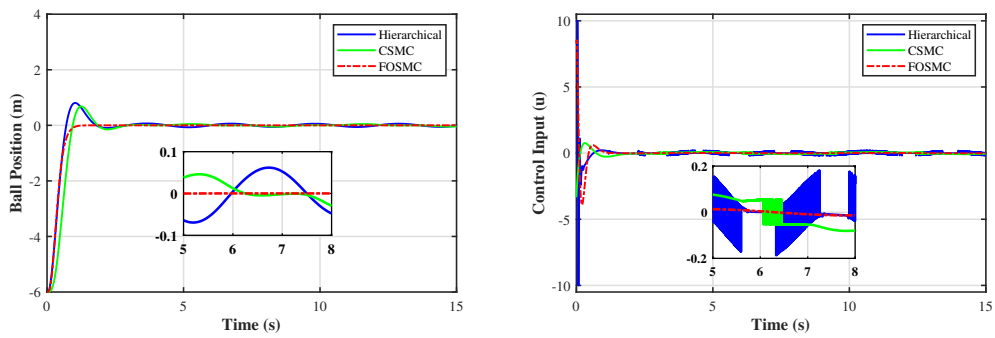

(**a**) (**b**)

Figure 5. Response curves of the BPS under the influence of parametric variations (Simulation Case 2): (**a**) Ball position. (**b**) Control input.

Case 3: In the third test, the disturbance rejection capability of the controllers was evaluated by applying a step disturbance at $t = 6$ s after the system had reached the equilibrium position. The corresponding ball position and control input responses are shown in Figure 6a and Figure 6b, respectively. As shown in Figure 6a, all controllers reject the applied disturbance and restore the ball position to the equilibrium point. However, the proposed FOCSMC exhibits the smallest deviation from the equilibrium position and achieves a faster recovery compared with the HSMC and the CSMC. The corresponding control input in Figure 6b remains smooth and bounded throughout the disturbance rejection process. The quantitative results reported in Table 3 further demonstrate the disturbance rejection capability of the proposed controller. The FOCSMC achieves an RMS and the MAX of 0.0011 cm and 0.0055 cm, respectively, whereas the HSMC yields 0.0292 cm

and 0.1440 cm, and the CSMC records 0.1408 cm and 0.5957 cm. These results indicate that the proposed controller maintains accurate regulation performance in the presence of external disturbances.

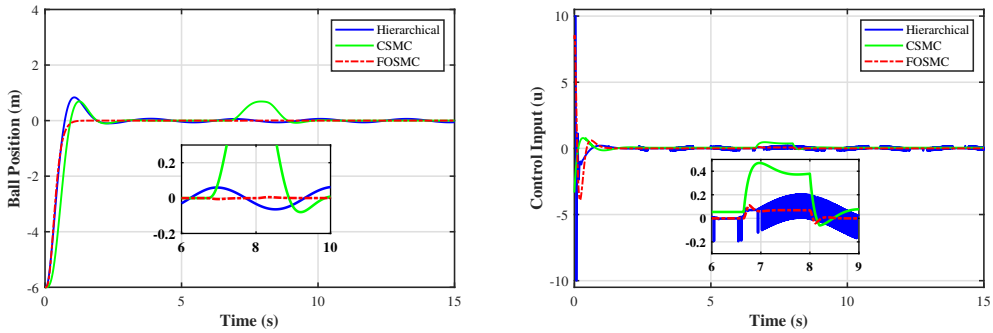

(**a**) (**b**)

Figure 6. Response curves of the BPS under the influence of external disturbance (Simulation Case 3): (**a**) Ball position. (**b**) Control input.

4.2. Experimental Results Analysis

Experimental results under different operating conditions are presented in this section. The proposed control schemes are validated on a two-degrees-of-freedom 2-DOF Quanser BPS as shown in Figure 7, which is widely used as a benchmark platform for evaluating nonlinear control algorithms [30]. The experimental setup consists of a square plate actuated by two orthogonally mounted Quanser SRV02 rotary servo motors that control the plate inclination about the x- and y-axes. Each servo is equipped with an optical encoder for real-time measurement of the motor position.

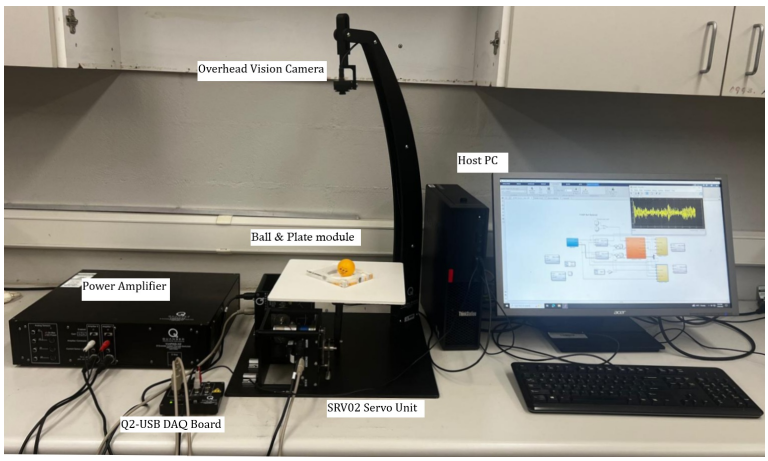

Figure 7. Experimental setup of the underactuated ball and plate system used for real-time validation.

The ball position is measured using an overhead digital camera mounted above the plate using Grey FlyCapture2 software, version 2.13.3.61. The camera operates at a resolution of 428 × 428 pixels and continuously captures the ball motion over the entire workspace. The acquired images are processed in MATLAB 2024b to estimate the ball coordinates, which are then used as feedback signals for closed-loop control. Further details on vision-based ball and plate control systems and the effects of sampling and camera delays can be found in [14,30].

The sensing and actuation components are interfaced with a PC through a Quanser Q2-USB data acquisition DAQ board. Control commands generated in MATLAB/Simulink are executed in real time using the QUARC platform. The DAQ board sends control voltages to the servo motors through a Quanser VoltPAQ-X2 amplifier while simultaneously

acquiring encoder measurements, enabling real-time closed-loop implementation of the proposed controllers.

This section presents experimental studies conducted on the BPS under various operating conditions to assess the effectiveness and robustness of the proposed FOCSMC.

Case 1: In the first experiment, the ball was initially positioned at −6 cm from the plate center, and the controllers were tasked with regulating it to the equilibrium position under nominal conditions. The resulting ball position and control-input responses are presented in Figure 8a and Figure 8b, respectively. As illustrated in Figure 8a, all three controllers successfully drive the ball toward the desired position. Nevertheless, the proposed FOCSMC exhibits a more rapid transient response and reaches the equilibrium point with noticeably smaller oscillations. In addition, the control effort shown in Figure 8b remains smoother and less fluctuating throughout the regulation process. The numerical results listed in Table 4 further highlight the advantages of the proposed approach. The FOCSMC achieves the smallest RMS error 0.0842 cm and the maximum error 0.1091 cm, outperforming the HSMC at 0.2379 cm and 0.4041 cm and the CSMC at 0.2426 cm 0.3814 cm. These observations indicate that the proposed controller provides more accurate regulation while maintaining a smoother control action under nominal operating conditions.

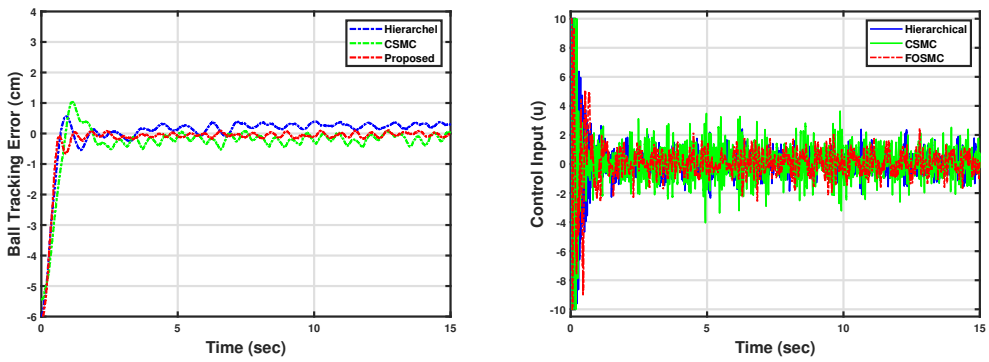

(**a**) (**b**)

Figure 8. Response curves of the BPS with the nominal system parameters (Experimental Case 1): (**a**) Ball position. (**b**) Control input.

Table 4. Experimental error analysis in (cm).

Controller	Index	Case 1	Case 2	Case 3
Proposed	RMS	0.0842	0.1049	0.5653
	MAX	0.1091	0.2563	1.9461
CSMC	RMS	0.2426	0.3700	0.7162
	MAX	0.3814	0.6672	2.4549
HSMC	RMS	0.2379	0.2401	1.0812
	MAX	0.4041	0.5141	3.3323

Case 2: To investigate the robustness against model uncertainty, the nominal ball was replaced with another ball whose physical properties increased the overall inertia by approximately 20%, thereby altering the system dynamics. The corresponding ball position and control-input responses are depicted in Figure 9a,b. Despite the parameter mismatch, stable operation is preserved for all controllers. However, the transient behavior differs considerably. The proposed FOCSMC maintains the ball trajectory closer to the equilibrium point and suppresses oscillatory motion more effectively than the benchmark controllers. Furthermore, the generated control signal remains bounded and free from excessive fluctuations throughout the experiment. A quantitative comparison is provided

in Table 4. The proposed method records the RMS and the maximum errors of 0.1049 cm and 0.2563 cm, respectively, whereas the HSMC produces 0.2401 cm and 0.5141 cm, and the CSMC yields 0.3700 cm and 0.6672 cm. These results demonstrate that the proposed controller retains its regulation capability even when the system parameters deviate from their nominal values.

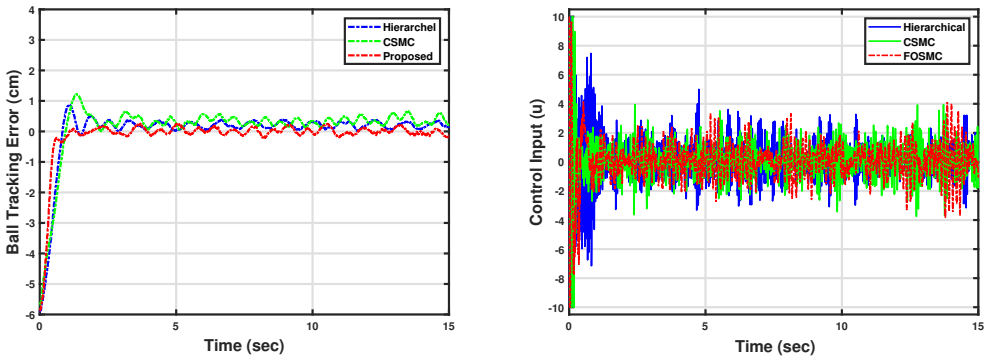

(**a**) (**b**)

Figure 9. Response curves of the BPS under the influence of parametric variations (Experimental Case 2): (**a**) Ball position. (**b**) Control input.

Case 3: The third experiment examines the ability of the controllers to recover from external disturbances. After the ball reached the equilibrium position, a step disturbance was introduced into the system. The resulting responses are shown in Figure 10a,b. The disturbance causes a temporary displacement of the ball from the desired position for all control schemes. However, the response obtained with the FOCSMC is characterized by a smaller excursion and a quicker return to equilibrium. Moreover, the corresponding control signal remains within acceptable bounds while effectively compensating for the disturbance. The superiority of the proposed strategy is also reflected in the performance metrics summarized in Table 4. The FOCSMC achieves the RMS and the maximum errors of 0.5653 cm and 1.9461 cm, respectively, compared with 1.0812 cm and 3.3323 cm for the HSMC and 0.7162 cm and 2.4549 cm for the CSMC. Hence, the proposed controller exhibits stronger disturbance attenuation and restores the system to its equilibrium state with improved precision.

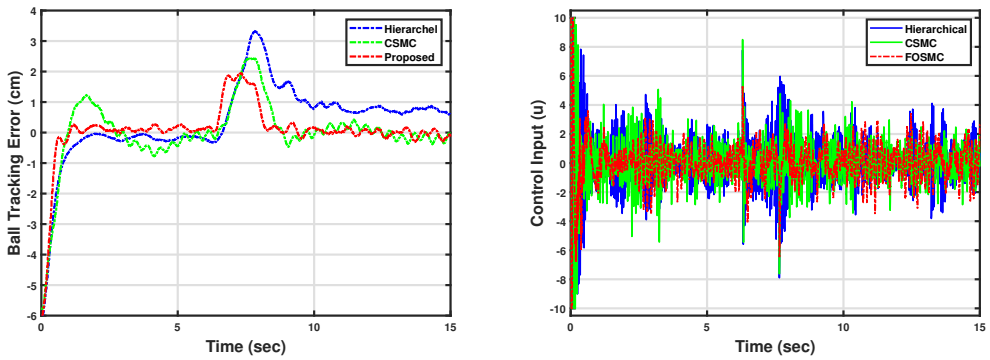

(**a**) (**b**)

Figure 10. Response curves of the BPS under the influence of external disturbance (Experimental Case 3): (**a**) Ball position. (**b**) Control input.

To summarize the results presented above, the proposed FOCSMC consistently achieves improved regulation performance under nominal conditions, parameter variations, and external disturbances. The continuous full-order sliding manifold effectively

reduces the chattering phenomenon commonly observed in conventional sliding mode control while preserving the robustness properties of the control scheme. In addition, the use of reduced-order state differentiators eliminates the need for direct high-order differentiation of measured signals, thereby reducing noise amplification and facilitating practical implementation on the experimental platform. The comparative simulation and experimental results demonstrate that the proposed controller provides faster convergence, smaller regulation errors, and smoother control inputs than the HSMC and the CSMC approaches. Furthermore, satisfactory regulation performance is maintained in the presence of parameter uncertainties and external disturbances, confirming the robustness and practical applicability of the proposed control strategy.

Case 4: To further demonstrate the two-dimensional (2-D) trajectory tracking capability of the ball under the proposed controller, a circular reference trajectory is used and generated by applying sinusoidal reference signals in both the x- and y-axis, as defined by $x_d(t) = R\cos(2\pi f_1 t)$ to track sinusoidal trajectory in the X-direction, while the ball tracks the sinusoidal $y_d(t) = R\sin(2\pi f_2 t)$ trajectory in the Y-direction, where $R = 0.04$ cm and $f_1 = f_2 = 0.5$ Hz.

Figure 11 shows the ball responses with the proposed scheme, in which Figure 11a,b are the tracking responses of the ball for the cosine trajectory in the X-direction and the sine trajectory in the Y-direction, respectively. We can see from Figure 11 that the actual response accurately follows the desired trajectory, while retaining the tracking error close to zero after the initial transient. In addition, the associated control input also is bounded and smooth, demonstrating the stable operation of the proposed controller in both axes.

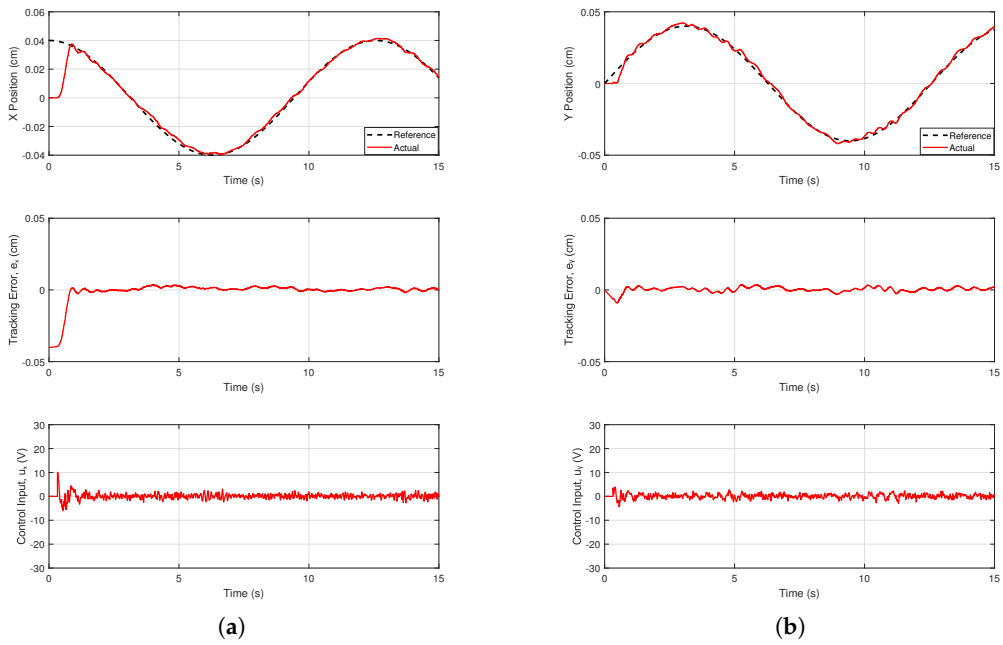

Figure 11. Experimental 2-D tracking performance for sinusoidal reference trajectories. (**a**) Ball position X, tracking error e_x and control input u_x along the x-axis from top to bottom. (**b**) Ball position Y, tracking error e_y and control input u_y along the y-axis from top to bottom (Experimental Case 4).

Accordingly, the overall 2-D tracking performance of the ball on the plate is illustrated in Figure 12, in which the reference and actual trajectories of the circular path are plotted in the X-Y plane. It is found that the ball under the proposed controller successfully and accurately tracks the circular trajectory, demonstrating its control capability to simultaneously regulate both axes and effectively handle the coupled dynamics of the underactuated BPS system in both axes.

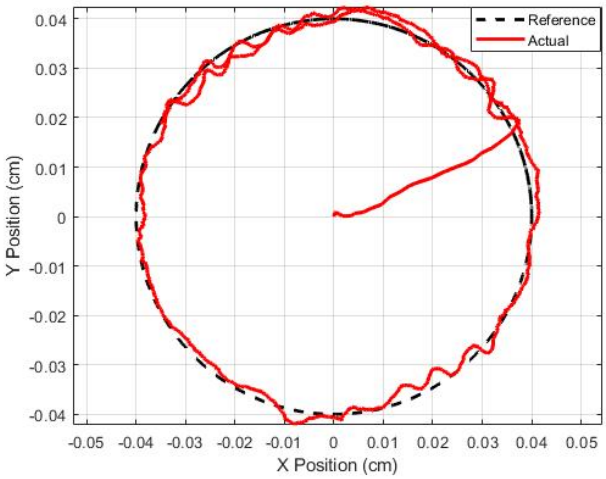

Figure 12. Two-dimensional trajectory tracking performance for the circular reference trajectory in the x–y plane (Experimental Case 4).

Remark 5. *The practical implementation of the BPS is affected by camera vision, sampling delay, coupling between the x-y axes, rolling friction, actuator input saturation, and so forth. To address the challenge of the noise caused by camera vision and position sensor, two cascade state differentiators in (9) and (10) reconstruct the unavailable velocity states from measured position signals without using direct numerical differentiations, thereby reducing the influence of measurement noise. The proposed robust FOCSMC in (18) compensates for coupling effects, model uncertainties, and external disturbances, while its continuous control action suppresses chattering. The successful simulation and experimental results demonstrate the effectiveness and practicality of the proposed approach for the actual implementation to the BPS. Addressing other challenges will be our future work, along with applying the advanced control methodologies.*

5. Conclusions

This paper presents a robust FOCSMC framework for the trajectory tracking of an underactuated BPS. By using a flatness-based canonical transformation, two SDs, and the CSMC, the proposed approach provides a practical and robust solution under different working conditions of the BPS. A Lyapunov-based analysis establishes asymptotic convergence of the tracking errors and asymptotic stability of the closed-loop of the BPS system. The proposed controller was successfully validated through simulation and experiments under nominal conditions, parameter variations, external disturbances, and 2-D circular trajectory tracking. Comparative results demonstrated superior tracking accuracy, smoother control effort, and enhanced robustness compared with the HSMC and the CSMC schemes. Under the hard experimental condition of the disturbance application, the proposed controller achieves an RMS and MAX tracking error of 0.5653 and 1.9461 cm, compared with 0.7162 and 2.4549 cm and 1.0812 and 3.3323 cm for the CSMC and the HSMC methods, respectively, confirming its effectiveness and practical applicability for underactuated BPSs. Future work will investigate the integration of evolutionary computing techniques, such as particle swarm optimization, genetic algorithms, and grey wolf optimizer, for systematic tuning of the controller parameters and further enhancement of the proposed methodology.

Author Contributions: Conceptualization, M.H.O. and K.R.; Methodology, M.H.O., K.R. and Z.C.; Software, M.H.O.; Validation, M.H.O., K.R. and Z.C.; Formal analysis, M.H.O. and K.R.; Investigation, K.R.; Resources, Z.C.; Writing—original draft, M.H.O. and K.R.; Writing—review & editing, K.R. and Z.C.; Supervision, Z.C. and Z.M.; Project administration, Z.C. and Z.M.; Funding acquisition, Z.C. and Z.M. All authors have read and agreed to the published version of the manuscript.

Funding: This research was supported by the Australian Research Council (ARC) through the Discovery Project Grant DP190101557.

Informed Consent Statement: Not applicable.

Data Availability Statement: The original contributions presented in this study are included in the article. Further inquiries can be directed to the corresponding author.

Conflicts of Interest: The authors declare that they have no conflicts of interest related to this work.

References

1. Spacek, L.; Vojtesek, J.; Gazdos, F. Control of Unstable Systems Using a 7 DoF Robotic Manipulator. *Machines* **2022**, *10*, 1164. [CrossRef]
2. Le, H.D.; Nestorovic, T. Second-Order Nonsingular Terminal Sliding Mode Control for Tracking and Stabilization of Cart–Inverted Pendulum. *Machines* **2026**, *14*, 111. [CrossRef]
3. Olfati-Saber, R. Nonlinear Control of Underactuated Mechanical Systems with Application to Robotics and Aerospace Vehicles. Ph.D. Thesis, Massachusetts Institute of Technology, Cambridge, MA, USA, 2001.
4. Kumar, D.T.R.; Mija, S.J. Multiswitching Surface Based Sliding Mode Controller for a Class of Underactuated Nonlinear Systems: With Application to Ball and Plate System. *IEEE Trans. Ind. Electron.* **2024**, *71*, 11326–11337. [CrossRef]
5. Debono, D.; Bugeja, M. Application of Sliding Mode Control to the Ball and Plate Problem. In Proceedings of the 12th International Conference on Informatics in Control, Automation and Robotics (ICINCO), Colmar, France, 21–23 July 2015; Volume 1, pp. 412–419.
6. Rsetam, K.; Cao, Z.; Man, Z. Design of Robust Terminal Sliding Mode Control for Underactuated Flexible Joint Robot. *IEEE Trans. Syst. Man Cybern. Syst.* **2021**, *52*, 4272–4285.
7. Khan, R.F.A.; Rsetam, K.; Cao, Z.; Man, Z. Singular Perturbation-Based Adaptive Integral Sliding Mode Control for Flexible Joint Robots. *IEEE Trans. Ind. Electron.* **2022**, *70*, 10516–10525.
8. Khan, R.F.A.; Rsetam, K.; Cao, Z.; Man, Z. Robust Continuous Terminal Sliding Mode Control for Flexible Joint Manipulators With Singular Perturbation. *Int. J. Robust Nonlinear Control* **2026**. [CrossRef]
9. Martins, L.; Cardeira, C.B.; Oliveira, P.J.R. Feedback Linearization with Zero Dynamics Stabilization for Quadrotor Control. *J. Intell. Robot. Syst.* **2020**, *101*, 7. [CrossRef]
10. Huang, J.; Wang, W.; Zhou, J. Adaptive Control Design for Underactuated Cranes with Guaranteed Transient Performance: Theoretical Design and Experimental Verification. *IEEE Trans. Ind. Electron.* **2021**, *69*, 2822–2832.
11. Ma, J.; Tao, H.; Huang, J. Observer Integrated Backstepping Control for a Ball and Plate System. *Int. J. Dyn. Control* **2021**, *9*, 141–148. [CrossRef]
12. Zarzycki, K.; Lawrynczuk, M. Fast Real-Time Model Predictive Control for a Ball-on-Plate Process. *Sensors* **2021**, *21*, 3959. [CrossRef] [PubMed]
13. Liu, Z.-G.; Wu, Y.-Q. Modeling and Adaptive Tracking Control for Flexible Joint Robots with Random Noises. *Int. J. Control* **2014**, *87*, 2499–2510. [CrossRef]
14. Ho, M.-T.; Rizal, Y.; Chu, L. Visual Servoing Tracking Control of a Ball and Plate System: Design, Implementation and Experimental Validation. *Int. J. Adv. Robot. Syst.* **2013**, *10*, 1. [CrossRef] [PubMed]
15. Tudic, V.; Kralj, D.; Hoster, J.; Tropcic, T. Design and Implementation of a Ball-Plate Control System and Python Script for Educational Purposes in STEM Technologies. *Sensors* **2022**, *22*, 1875. [CrossRef] [PubMed]
16. Chang, Y.-H.; Chan, W.-S.; Chang, C.-W. TS Fuzzy Model-Based Adaptive Dynamic Surface Control for Ball and Beam System. *IEEE Trans. Ind. Electron.* **2012**, *60*, 2251–2263.
17. Shojaei, K. Neural Network Feedback Linearization Target Tracking Control of Underactuated Autonomous Underwater Vehicles with a Guaranteed Performance. *Ocean Eng.* **2022**, *258*, 111827. [CrossRef]
18. Yang, G. State Filtered Disturbance Rejection Control. *Nonlinear Dyn.* **2025**, *113*, 6739–6755. [CrossRef]
19. Yang, G. Multilayer Neuroadaptive Reinforcement Learning of Disturbed Nonlinear Systems via Actor–Critic Mechanism. *IEEE Trans. Autom. Sci. Eng.* **2025**, *23*, 1372–1381. [CrossRef]
20. Idrees, M.; Ullah, S.; Muhammad, S. Sliding Mode Control Design for Stabilization of Underactuated Mechanical Systems. *Adv. Mech. Eng.* **2019**, *11*, 1687814019842712. [CrossRef]
21. Yesmin, A.; Sinha, A. Sliding Mode Controller for Quadcopter UAVs: A Comprehensive Survey. *Drones* **2025**, *9*, 625. [CrossRef]
22. Ginoya, D.; Shendge, P.D.; Phadke, S.B. Disturbance Observer Based Sliding Mode Control of Nonlinear Mismatched Uncertain Systems. *Commun. Nonlinear Sci. Numer. Simul.* **2015**, *26*, 98–107. [CrossRef]

23. Rsetam, K.; Afsar, R.F.; Cao, Z.; Man, Z. Performance Analysis of Finite-Time Generalized Proportional Integral Observer for Uncertain Brunovsky Systems. In Proceedings of the 2023 International Conference on Advanced Mechatronic Systems (ICAMechS), Melbourne, Australia, 4–7 September 2023; pp. 1–6.
24. Dil Kumar, T.R.; Mija, S.J. Synthesis and Experimental Demonstration of a Hybrid Adaptive PID-SMC Algorithm for a Class of Underactuated Nonlinear Systems. *Nonlinear Dyn.* **2025**, *113*, 15037–15056. [CrossRef]
25. Singh, R.; Bhushan, B. Condition Monitoring Based Control Using Wavelets and Machine Learning for Unmanned Surface Vehicles. *IEEE Trans. Ind. Electron.* **2020**, *68*, 7464–7473. [CrossRef]
26. Wang, H.; Zhang, Q.; Sun, Z.; Tang, X.; Chen, I.-M. Continuous Terminal Sliding-Mode Control for FJR Subject to Matched/Mismatched Disturbances. *IEEE Trans. Cybern.* **2021**, *52*, 10479–10489. [CrossRef] [PubMed]
27. Ali, K.; Cao, Z.; Rsetam, K.; Man, Z. Robust Adaptive Integral Fast Sliding Mode Control for Servo Motors. *Mechatronics* **2026**, *117*, 103504. [CrossRef]
28. Qian, D.; Yi, J. *Hierarchical Sliding Mode Control for Under-Actuated Cranes*; Springer: Berlin/Heidelberg, Germany, 2016.
29. Quanser Inc. *Ball and Plate System–Instructor Manual*; Quanser Inc.: Markham, ON, Canada, 2018.
30. Wang, H.; Vasseur, C.; Christov, N.D.; Koncar, V. Vision Servoing of Robot Systems Using Piecewise Continuous Controllers and Observers. *Mech. Syst. Signal Process.* **2012**, *33*, 132–141. [CrossRef]
31. Khan, R.F.A.; Rsetam, K.; Cao, Z.; Man, Z. ESO Based Adaptive Fixed-Time Integral Sliding Mode Control for Flexible Joint Robots Using Singular Perturbation Method. *Nonlinear Dyn.* **2025**, *113*, 24981–25000. [CrossRef]
32. Li, Y.; Xu, Q. Adaptive Sliding Mode Control with Perturbation Estimation and PID Sliding Surface for Motion Tracking of a Piezo-Driven Micromanipulator. *IEEE Trans. Control Syst. Technol.* **2009**, *18*, 798–810. [CrossRef]

Disclaimer/Publisher's Note: The statements, opinions and data contained in all publications are solely those of the individual author(s) and contributor(s) and not of MDPI and/or the editor(s). MDPI and/or the editor(s) disclaim responsibility for any injury to people or property resulting from any ideas, methods, instructions or products referred to in the content.